ELSEVIER

Journal of Fluids and Structures 24 (2008) 541–558

JOURNAL OF FLUIDS AND STRUCTURES

www.elsevier.com/locate/jfs

Experimental investigation of dynamic stability of a cantilever pipe aspirating fluid

G.L. Kuiper[a,*], A.V. Metrikine[b]

[a]Shell International Exploration and Production, P.O. Box 60, 2280 AB Rijswijk, The Netherlands
[b]Faculty of Civil Engineering and Geosciences, Delft University of Technology, P.O. Box 5048, 2600 GA Delft, The Netherlands

Received 11 December 2006; accepted 24 October 2007
Available online 20 December 2007

Abstract

The dynamic stability of a submerged cantilever pipe conveying fluid from the free end to the fixed one is considered as one of the unresolved issues in the area of fluid–structure interaction. There is a contradiction between theoretical predictions and experiments. Reported experiments did not show any instability, while theory predicts instability beyond a critical fluid velocity. Recently, several papers appeared, improving the theoretical modelling of pipe dynamics. All theories predict instability, either oscillatory or static, referred to here as flutter and divergence, respectively. A new test set-up was designed to investigate the hypothesis that previous experimental set-ups could not allow observations of pipe instability or the pipe aspirating water is unconditionally stable. In this new test set-up, the fluid velocity could exceed the theoretically predicted critical velocities. A cantilever pipe of about 5 m length was partly submerged in water. The free open end of the pipe was in the water, whereas the fixed end was above the waterline. The experiments clearly showed that the cantilever pipe aspirating water is unstable beyond a critical velocity of water convection through the pipe. Below this velocity the pipe is stable, whereas above it the pipe shows a complex motion that consists of two alternating phases. The first phase is a nearly periodic orbital motion with maximum amplitude of a few pipe diameters, whereas the second one is a noise-like vibration with very small amplitudes. Increasing the internal fluid velocity results in a larger amplitude of the orbital motion, but does not change the pipe motion qualitatively.

Keywords: Cantilever pipe; Stability; Experiments; Fluid–structure interaction; Flutter

1. Introduction

Most studies of dynamic stability of a cantilever pipe conveying fluid are devoted to pipes discharging the fluid from the free end. A comprehensive overview of these studies can be found in Païdoussis (1998). For fluid velocities below a critical value, such pipes are stable, whereas at higher velocities they become unstable by flutter. Theoretical models predict the same critical velocity as observed in experiments.

The closely related problem of a submerged cantilever pipe aspirating water through its free end received much less attention in the past. There is no consensus among researchers as to the mechanism of instability and the magnitude of the fluid velocity beyond which the instability occurs. In a recent paper, Païdoussis (2005) classified this problem as one

*Corresponding author. Tel.: +31 70 447 3411; fax: +31 70 447 4503.
E-mail address: Guido.Kuiper@shell.com (G.L. Kuiper).

0889-9746/$ - see front matter
doi:10.1016/j.jfluidstructs.2007.10.011

of the unresolved issues in the area of fluid–structure interactions. A number of experiments were carried out in the past (Hongwu and Junji, 1996; Païdoussis, 1998) in order to experimentally observe and study the instability. However, in all these experiments the pipe remained stable. In contrast to this, the early theoretical models, neglecting energy loss on the pipe motion in a surrounding fluid, predicted instability at infinitesimal fluid velocities (Païdoussis and Luu, 1985). In attempts to explain this contradiction, several papers appeared recently, improving the theoretical modelling of a cantilever pipe aspirating fluid:

1. Païdoussis (1999) suggested an improved description of the negative pressurization of water at the inlet of the pipe. However, this appeared to have but a small effect on the stability of the cantilever.
2. Kuiper and Metrikine (2005) and Kuiper et al. (2007) showed that the external hydrodynamic drag is a major stabilizing factor, which is likely to prohibit the pipe instability at the speeds reached in the experiments.
3. Païdoussis et al. (2005) postulated several new descriptions of the boundary condition for the balance of transverse forces at the free end of the pipe. The basic description of this boundary condition in this paper assumes that the inflow remains nearly tangential to the undeflected pipe. Using this boundary condition, the pipe is predicted to lose stability by divergence at a non-zero fluid speed.

Despite some differences, all improved theories still suggest that the pipe should become unstable, in one way or another, at a certain fluid speed. Thus, it remained unclear whether the previous experimental set-ups did not allow to observe the instability, or whether the pipe aspirating water is unconditionally stable and all existing theories have to be improved further.

No instability was observed in any experiment we are aware of. In the experiment of Hongwu and Junji (1996) a 1 m length pipe with an internal diameter of 8.2 mm was used. The velocity of fluid flow through the pipe was relatively low due to the small diameter of the pipe (high internal wall friction) and the capacity of the pump. For the maximum attainable flow rate, no flutter was observed. In the book of Païdoussis (1998) it is mentioned that the author conducted small-scale experiments with an elastomer pipe; however, exact dimensions of the test set-up are not given. Flutter was not observed at small flow velocities. After increasing the flow rate, local shell-type collapse of the pipe near the support was observed owing to the underpressure in the pipe. Hence, in all experiments known to us, no sign of global instability was observed.

The aim of the present paper is to investigate whether the instability of a pipe aspirating fluid can be observed experimentally and if so, to compare the observational results to theoretical predictions. To this end, we have built a test set-up in which the fluid velocity through the pipe could exceed all predicted critical velocities of the above-mentioned theories. A cantilever pipe of about 5 m long with a diameter of about 0.1 m was partly submerged in water. The internal fluid velocity could reach a value of nearly 7 m/s.

This paper reports some observations made using this set-up and is structured as follows. In Section 2, existing theories are briefly discussed and critical velocities are computed according to these theories. The description of the experimental set-up is given in Section 3. The observed pipe behaviour is described qualitatively and quantitatively in Sections 4 and 5, respectively. In Section 6, the observed critical velocity and the measured frequency of the pipe motion are compared to existing theory (Païdoussis et al., 2005; Kuiper et al., 2007). Since both the critical velocity and the pipe behaviour in the unstable regime are not predicted with existing theory, some possible improvements of the theory are suggested in Section 7.

2. Critical velocities predicted by different theories

In this section several theoretical models of an initially straight, submerged pipe aspirating fluid are briefly summarized. The models differ mainly in the description of the boundary condition at the free inlet. Using the Argand diagram (Païdoussis, 1998), the critical velocities and the type of instability are examined. The experimental set-up is designed such that these velocities can be achieved.

The pipe is considered to be slender, its two transverse deflections, $v(z,t)$ and $w(z,t)$, to be small compared to the length of the pipe, and the vibrations to be of a low frequency, so that the Euler–Bernoulli theory is applicable for the description of the pipe dynamic bending. In this section, the effective tension, the material damping and the effect of depressurization at the inlet are disregarded as having minor effect on the pipe stability (the tension can be neglected because an almost neutrally buoyant pipe is used in the experiments). The two coupled equations of the transverse motion of the submerged pipe subjected to a nonlinear hydrodynamic drag read (Païdoussis et al., 2005; Kuiper et al., 2007):

$$EI\frac{\partial^4 v}{\partial z^4} - 2m_f u_f \frac{\partial^2 v}{\partial z\,\partial t} + m_f u_f^2 \frac{\partial^2 v}{\partial z^2} + M\frac{\partial^2 v}{\partial t^2} + D_o\left(\frac{\mu}{D_o}A_1\frac{\partial v}{\partial t} + \frac{1}{2}\rho_f A_2 \frac{\partial v}{\partial t}\sqrt{\left(\frac{\partial v}{\partial t}\right)^2 + \left(\frac{\partial w}{\partial t}\right)^2}\right) = 0, \tag{1}$$

$$EI\frac{\partial^4 w}{\partial z^4} - 2m_f u_f \frac{\partial^2 w}{\partial z\,\partial t} + m_f u_f^2 \frac{\partial^2 w}{\partial z^2} + M\frac{\partial^2 w}{\partial t^2} + D_o\left(\frac{\mu}{D_o}A_1\frac{\partial w}{\partial t} + \frac{1}{2}\rho_f A_2 \frac{\partial w}{\partial t}\sqrt{\left(\frac{\partial v}{\partial t}\right)^2 + \left(\frac{\partial w}{\partial t}\right)^2}\right) = 0, \tag{2}$$

in which z is the coordinate along the pipe axis, t the time, EI the bending stiffness, m_f the internal fluid mass per unit length, M the summation of added mass, mass of the pipe and mass of the internal fluid, all per unit length, u_f the fluid velocity, D_o the outer diameter of the pipe, μ the dynamic viscosity of the fluid, ρ_f the fluid density and A_1 and A_2 are constants. The two terms in the brackets represent the linear and quadratic damping caused by the surrounding fluid (Kuiper et al., 2007), that is assumed quiescent.

The onset of instability is governed by the linearized equations of motion. Linearization of Eqs. (1) and (2) results in two identical equations for $w(z, t)$ and $v(z, t)$. Hence, for analysing the onset of instability it is sufficient to consider only the equation of motion in one plane:

$$EI\frac{\partial^4 w}{\partial z^4} - 2m_f u_f \frac{\partial^2 w}{\partial z\,\partial t} + m_f u_f^2 \frac{\partial^2 w}{\partial z^2} + M\frac{\partial^2 w}{\partial t^2} + \mu A_1 \frac{\partial w}{\partial t} = 0. \tag{3}$$

The difference between several theoretical models is related to the balance of transverse forces at the free inlet. All models use a zero bending moment at this inlet. The conventional boundary condition assumes a zero shear force at the free end (Païdoussis, 1998,1999; Kuiper and Metrikine, 2005):

$$EI\frac{\partial^3 w}{\partial z^3} = 0 \quad \text{at} \quad z = L. \tag{4}$$

In a recent paper, Païdoussis et al. (2005) postulated new descriptions for the force balance at the free end. We highlight here only two of these descriptions, although alternative variants were discussed in Païdoussis et al. (2005) by varying the assumptions concerning depressurization, tension and inflow direction. Two relationships were introduced for the force balance at the free end:

$$EI\frac{\partial^3 w}{\partial z^3} - m_f u_f\left(\frac{\partial w}{\partial t} - u_f\frac{\partial w}{\partial z}\right) = 0 \quad \text{at} \quad z = L, \tag{5}$$

$$EI\frac{\partial^3 w}{\partial z^3} - m_f u_f \frac{\partial w}{\partial t} = 0 \quad \text{at} \quad z = L. \tag{6}$$

To explain the physical differences between the descriptions, three sketches are shown in Fig. 1. Inside the pipe the internal fluid velocity u_f and the horizontal pipe velocity $\partial w/\partial t$ are indicated with a regular arrow. The dotted arrow inside the pipe marks the resultant direction of water at the entrance. Obviously, the arrows inside the pipe are the same for all three sketches. The differences originate from the assumptions regarding the flow field just below the entrance. The dotted arrow below the pipe represents the spatially averaged resultant direction of the flow field just below the entrance. Boundary condition (4) assumes the inflow direction be tangential to the *deflected* pipe and the inflow field to move with the same horizontal velocity as the tip of the pipe. As a result, the conventional boundary condition (4)

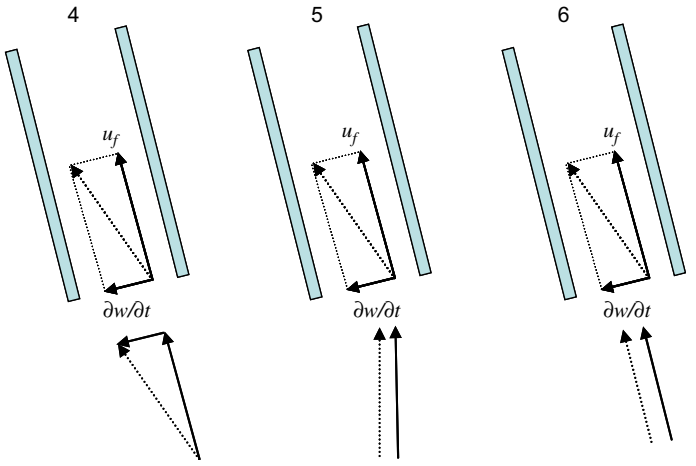

Fig. 1. Three sketches of inflow conditions corresponding to boundary conditions (4), (5) and (6).

presumes that the momentum of the fluid remains unchanged as the fluid enters the pipe. Boundary conditions (5) and (6) assume that the flow field just below the entrance does not move horizontally with the pipe, and hence the corresponding horizontal component is absent in these two sketches. This assumption results in a non-smooth flow field and, as a result, the momentum of the fluid changes as the fluid enters the pipe. The difference between boundary conditions (5) and (6) is that the former assumes a spatially averaged inflow direction tangential to the *undeflected* pipe, while the latter assumes the inflow direction tangential to the *deflected* pipe.

The dynamic stability of a linear system is determined by its eigenfrequencies. To find these, the displacement of the pipe can be sought for in the following form:

$$w(z,t) = W(z)\exp(\mathrm{i}\omega t), \tag{7}$$

where ω is the complex frequency. The system is stable if the imaginary parts of all eigenfrequencies are positive, and unstable if at least one eigenfrequency has a negative imaginary part. The most common way to analyse the eigenfrequencies is to make use of an Argand diagram. In this diagram the real and imaginary parts of the natural frequency ω are plotted parametrically, as they depend on one (or more) of the system parameters. Here the flow velocity u_f and the linear drag coefficient A_1 are used as such parameters. At the first step of the analysis, both the fluid velocity and the external damping are disregarded. The system possesses in this case only real natural frequencies, which can be easily found numerically. As the second step, the damping is gradually increased, keeping the velocity zero, and the accompanying complex values of the natural frequencies are computed and plotted in the Argand diagram. As expected, all complex natural frequencies acquire positive imaginary part, implying that the pipe is stable. Once the linear damping coefficient A_1 reaches the value for which the stability is studied, the fluid velocity is gradually increased from zero, keeping the value A_1 constant. As a result, the imaginary part of the complex natural frequencies decreases with increasing fluid velocity. At a certain velocity, the imaginary part of some natural frequencies becomes negative, implying that the pipe becomes unstable.

For the three above-mentioned boundary descriptions at the inlet, Eqs. (4)–(6), the Argand diagrams have been plotted in Figs. 2–4 using the parameters given in Table 1. These parameters correspond to a flexible plastic pipe of 4.75 m length fully submerged in water and are close to the dimensions of the actual experimental pipes. A relatively long pipe was needed to achieve a sufficiently high flexibility that would enable the instability. In Figs. 2–4 only the evolution of the first natural frequency is shown, since this frequency is the first to enter the lower half-plane. As can be seen from these figures, the three boundary conditions result in different critical fluid velocities and different types of instability:

(i) Eq. (4) results in a critical velocity of 7.86 m/s and predicts flutter beyond this velocity;
(ii) Eq. (5) results in a critical velocity of 5.05 m/s and predicts divergence beyond this velocity;
(iii) Eq. (6) results in a critical velocity of 10.6 m/s and predicts flutter beyond this velocity.

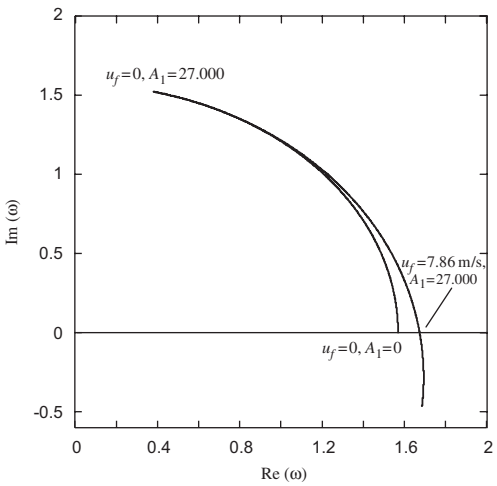

Fig. 2. Argand diagram for a fully submerged pipe according to boundary condition (4). In view of the diagram symmetry with respect to the vertical axis, only the right half-plane is shown.

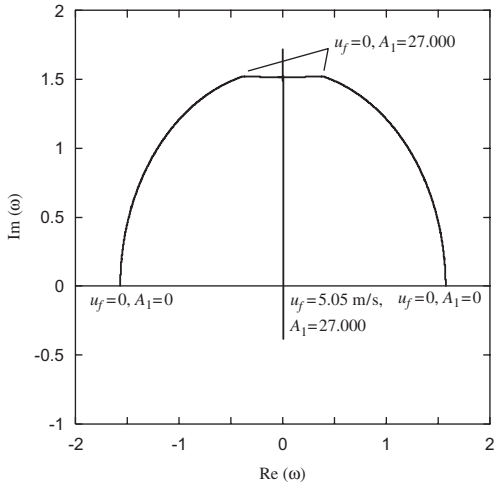

Fig. 3. Argand diagram for a fully submerged pipe according to boundary condition (5).

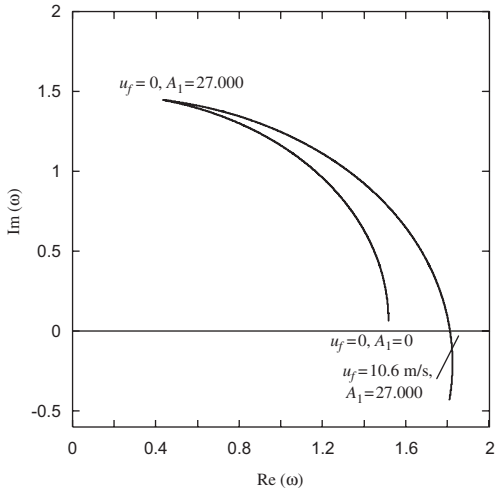

Fig. 4. Argand diagram for a fully submerged pipe according to boundary condition (6). In view of the diagram symmetry with respect to the vertical axis, only the right half-plane is shown.

Table 1
Parameters used for obtaining the Argand diagrams

Parameter			
E	2.40×10^9 N/m^2	ρ_f	1.00×10^3 kg/m^3
L	4.75 m	ρ_p	1.06×10^3 kg/m^3
D_o	0.075 m	C_a	1.00
D_i	0.070 m	μ	1.00×10^{-3} kg/m/s
$A_{1,\max}$	27.0×10^3		

To check which of the three predictions resembles reality, the experimental set-up should allow achieving the highest critical velocity predicted by Eq. (6). The difficulty in doing so was that it is impossible to steadily pump water through a pipe of 0.075 m diameter with a velocity higher than 7 m/s. This limit is set by wall friction and cavitation.

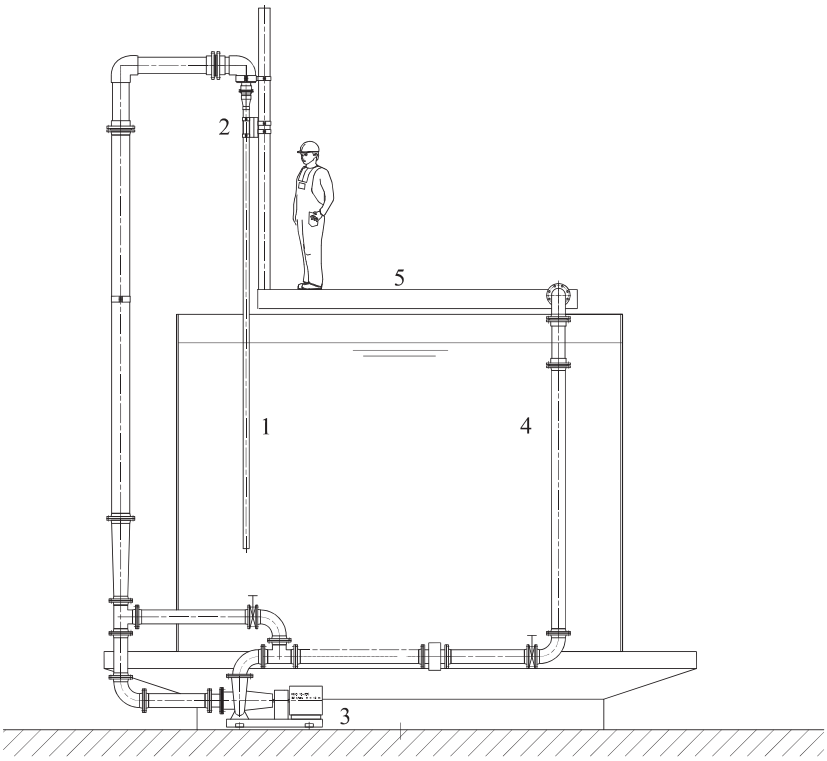

Fig. 5. Side view of the experimental set-up. (1) Partly submerged cantilever pipe, (2) rigid connection to stiff steel pipe, (3) centrifugal pump, (4) return pipe and (5) concrete balcony.

A solution was found in submerging only a part of the pipe. This reduced the hydrodynamic drag, and consequently, the critical velocities in the cases of flutter, predicted by Eqs. (4) and (6).

3. Experimental set-up and instrumentation

The experimental set-up, built at WL Delft Hydraulics in the Netherlands, consisted of a plastic pipe partly submerged in a tank of 6 m diameter filled with water, as shown in Figs. 5 and 6 (side view and top view). The free inlet of the pipe was 1.25 m above the bottom of the tank, so that the flow near the entrance was insignificantly affected by the bottom. The depth of water in the tank was 3.2 m. If needed, the water level inside the tank could be lowered, but we first focused on this level. In this situation the length of the submerged part of the pipe was 1.95 m. The top of the pipe was rigidly fixed to a stiff steel pillar mounted to a concrete balcony. Above this fixation the pipe widened to reduce the internal wall friction. A centrifugal pump was located outside the tank and the flow re-entered the tank through a return pipe at the other side. Two pipes of different diameter were tested. Their main parameters and the water parameters are given in Table 2. To give a better impression of the experimental set-up, a photograph of the 4.75 m long pipe in the dry tank is shown in Fig. 7.

For the smaller diameter pipe, the maximum internal fluid velocity we could reach was nearly 7.0 m/s. For this speed one could clearly hear that cavitation started to occur. And even worse, the underpressure in the plastic pipe was so high that the pipe buckled locally at the top; the circular shape of the cross-section became unstable. To avoid the latter, the top part of the pipe was stiffened on the outside by metallic rings. For the larger diameter pipe we could reach a maximum fluid velocity of 5.3 m/s, which was close to the discharge capacity of the pump. For this pipe, cavitation and local buckling was not an issue.

Although not desirable, the pipe axis was only 25 cm away from the wall of the tank. The practical reason was that in this case the top of the pipe could easily be fixed to the steel pillar mounted to the concrete balcony. Although the pipe was positioned at a distance of five times its radius from the wall, it seemed that the wall influence was not pronounced.

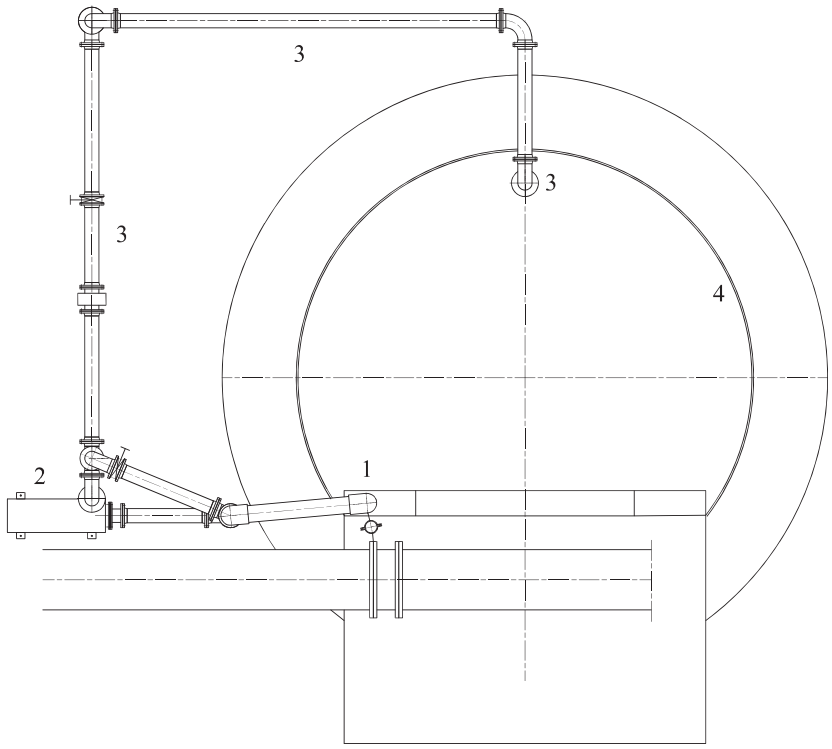

Fig. 6. Top view of the experimental set-up: (1) Cantilever pipe aspirating fluid, (2) centrifugal pump, (3) return pipe and (4) tank wall.

This statement is based on two observations. During several experimental runs we injected a blue ink to visualize the flow near the pipe entrance and near the wall. The ink clearly indicated that there were no wall-induced flow patterns between the pipe and the wall. Secondly, in the unstable regime the pipe showed a nearly circular orbital motion, while in the case of a strong wall influence a more elliptical one would have been expected. However, in future experiments the pipe will be located further away from the wall of the tank.

Two displacement transducers were installed to measure the transverse deflections of the pipe in two perpendicular directions. Since these transducers were non-contact (induction-based), they did not affect the pipe motion. They were installed at the balcony level and recorded the motion with a sampling frequency of 100 Hz. An underwater camera recorded the motion of the pipe near the tip. The water discharge was electromagnetically measured just downstream the centrifugal pump with a sampling frequency of 100 Hz. This signal showed a steady fluid discharge during the experiments. From the discharge we could easily calculate the fluid velocity through the cantilever pipe, assuming an incompressible fluid. The intention was to measure the water pressure at the top of the cantilever pipe. Unfortunately, the device meant to do so did not work properly.

4. Experimental observations—qualitative description

During the experiments the internal fluid velocity was gradually increased from zero to a desired velocity. For about 5 min the fluid velocity was kept constant before measurements were started. From the observations, two regimes could be distinguished. Below a certain critical fluid velocity the pipe remained stable, i.e. the pipe did not move. Exceeding this critical velocity, the pipe motion was observed in the form of a complex motion that consisted of two alternating phases: a nearly periodic orbital motion and a noise-like vibration with very small amplitudes. Usually noise-like vibrations were first observed during a few minutes before the pipe started to orbit. Then, the orbital motion started and lasted for about a few minutes. Thereafter, the orbital motion ceased to exist and noise-like vibrations were observed again, etc. (it should be emphasized that during an experimental run all parameters were kept constant). This alternating behaviour was observed for both pipes. There was no qualitative difference of the pipe behaviour observed

Fig. 7. Cantilever plastic pipe in the dry tank.

Table 2
Parameters of the experimental pipes and the fluid

Parameter	Smaller pipe	Larger pipe
E	2.70×10^9 N/m^2	2.20×10^9 N/m^2
L	4.75 m	4.66 m
L_{dry}	2.80 m	2.89 m
L_{subm}	1.95 m	1.77 m
D_o	0.075 m	0.110 m
D_i	0.070 m	0.104 m
ρ_f	1.00×10^3 kg/m^3	1.00×10^3 kg/m^3
ρ_p	1.06×10^3 kg/m^3	1.06×10^3 kg/m^3
C_a	1.6	1.4
μ	1.00×10^{-3} kg/m/s	1.00×10^{-3} kg/m/s
A_1	2.4×10^3	2.4×10^3
A_2	0.24	0.24
α	1.62 kg m/s	9.53 kg m/s
γ_e	0.5	0.5

for fluid velocities just above critical or for much larger flow velocities. In both cases the motion consisted of the two alternating phases: small, noise-like vibrations and orbital motion with displacements with order of magnitude of the pipe diameter. However, both the frequency and the amplitude of the orbital motion increased with fluid velocity. For the maximal attainable fluid velocity of 7.0 m/s, the orbital motion of the tip of the smaller diameter pipe had a radius of more than 1.5 times the pipe diameter. It was also observed that the pipe orbits always in the same direction. This may be due to a number of unknown asymmetries of the experimental set-up with respect to the pipe axis. Finally, it should be noted that we never observed a pure planar motion.

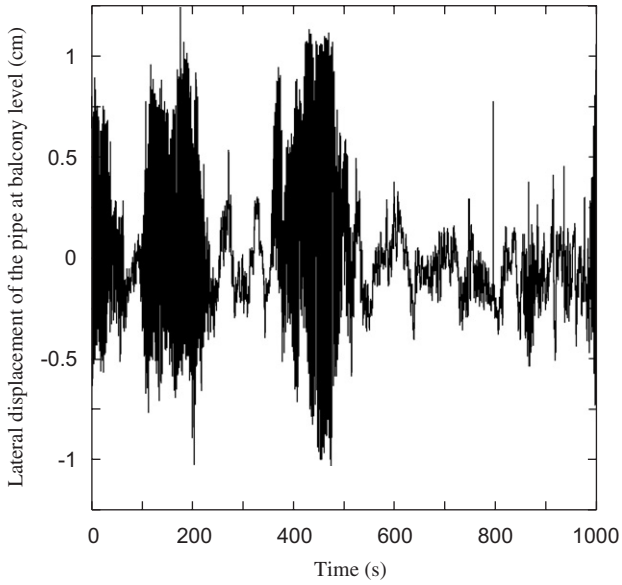

Fig. 8. *Y*-displacement of the smaller diameter pipe measured by the displacement transducer for a fluid velocity of 6.2 m/s.

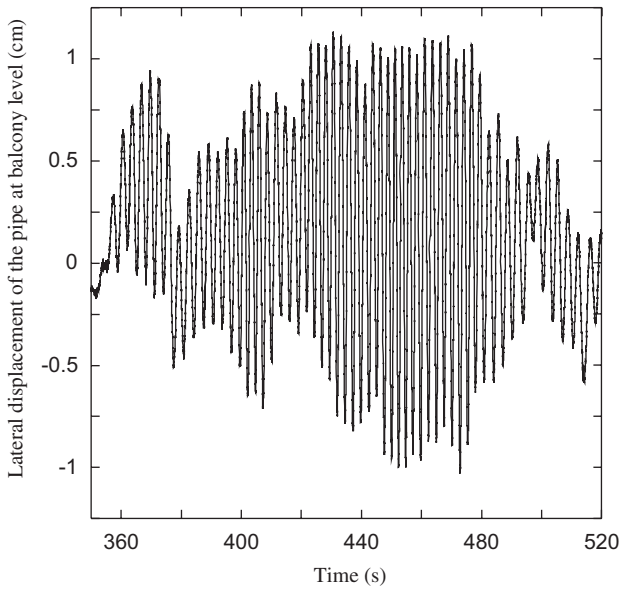

Fig. 9. A blow-up of Fig. 8 (350–520 s). In this regime an almost sinusoidal motion is measured.

5. Experimental observations—quantitative description

As a first step, the first natural bending frequency of the partly submerged pipes filled with still (not flowing) water was determined. The first natural frequency was identified for the situation that the lower 1.95 m of the pipe was

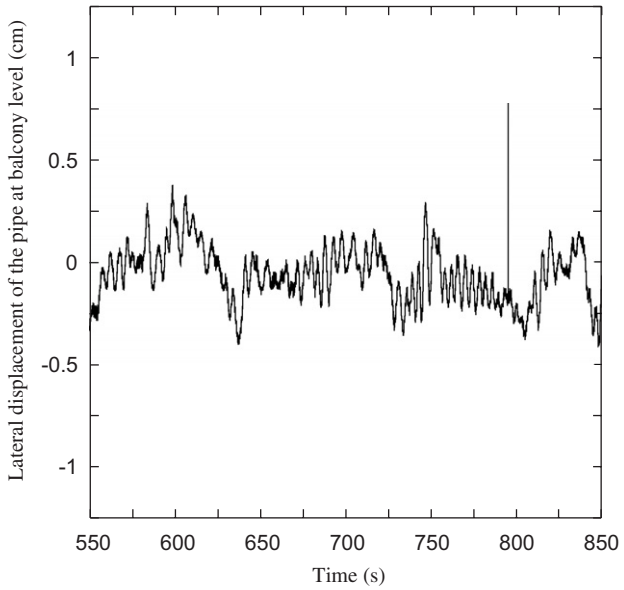

Fig. 10. A blow-up of Fig. 8 (550–850 s). In this regime the variations in amplitude are much smaller and the time signature of the displacement is not repetitive.

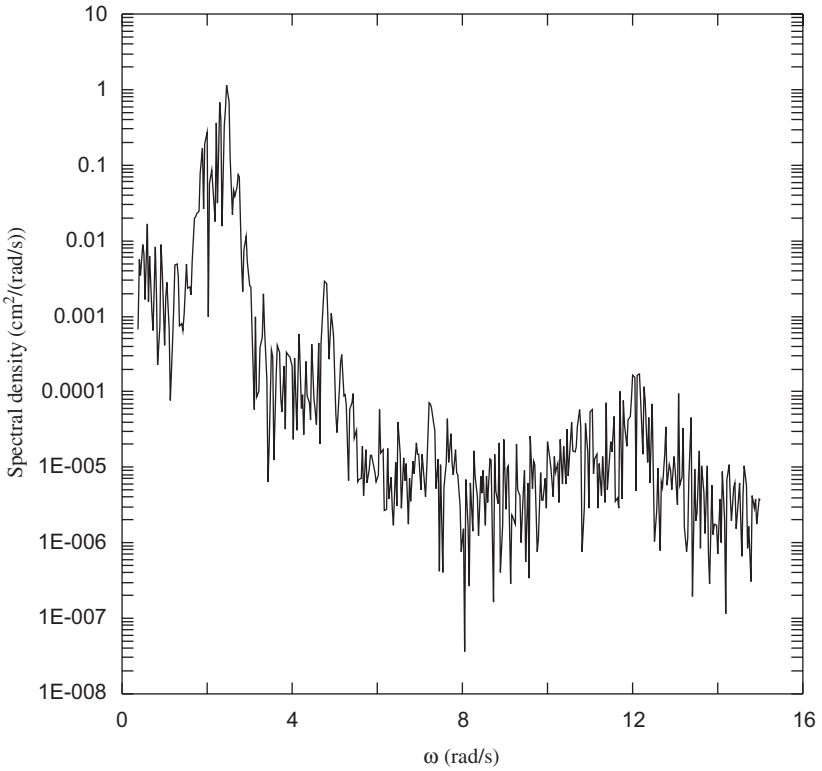

Fig. 11. *Y*-displacement spectrum based on Fig. 9 (orbital motion).

submerged. The pipe was given an initial deflection and then released. From the record of the pipe displacements, the period of free decaying vibrations was extracted and the natural frequencies were calculated. The first bending natural frequency for the smaller and larger diameter pipes filled with still water was 1.5 and 2.1 rad/s, respectively.

It is not easy to accurately determine the critical fluid velocity beyond which the pipe is unstable. The problem is that the motion that corresponds to the near-critical velocities is very small. Hence, the period of measurements needs to be long enough to determine whether the pipe exhibits orbital motion during some time. Looking at the data one could estimate that the smaller pipe ($D_o = 0.075$ m) exhibited orbital response starting from a velocity of 2.1–2.4 m/s. The larger pipe ($D_o = 0.11$ m) showed this behaviour from a velocity of 1.9–2.2 m/s. For the smaller pipe, the frequency of the orbital motion for fluid velocities just exceeding the critical velocity was around 1.6 rad/s, which is only slightly larger than the first natural frequency of the pipe filled with still water (1.5 rad/s for $u_f = 0$ m/s).

The most inexplicable observation for us was the alternating pipe motion for the fluid velocities in the post-critical regimes. As an example of the alternating pipe motion, a measured transverse displacement of the smaller diameter pipe is shown in Fig. 8. This displacement was measured at the balcony level, at a height of 3.17 m above the pipe tip, for a fluid velocity of 6.2 m/s. Figs. 9 and 10 are a blow-up of the displacements of the orbital motion (350–520 s) and of the noise-like vibrations (550–850 s), respectively. The spectra of both displacement records are shown in Figs. 11 and 12. It is interesting to see that in the spectrum of the orbital motion (Fig. 11) there is a clear peak around the first natural frequency of the pipe. In comparison with the situation when the water in the pipe is still, the natural frequency of the first bending mode increases from 1.5 rad/s ($u_f = 0$ m/s) to 1.6 rad/s ($u_f = 2.2$ m/s) and then to around 2.2 rad/s ($u_f = 6.2$ m/s). In the regime of noise-like vibrations this peak is completely absent (see Fig. 12). It was checked whether the spectra contained energy around the second or higher natural frequencies. This was hardly the case. The small amplification around 12 rad/s in Figs. 11 and 12 is related to the frequency of the second bending mode. Hence, the orbital motion originates mainly from the first bending mode instability. The smaller peak in Fig. 11 around 4.8 rad/s is explained in the next section.

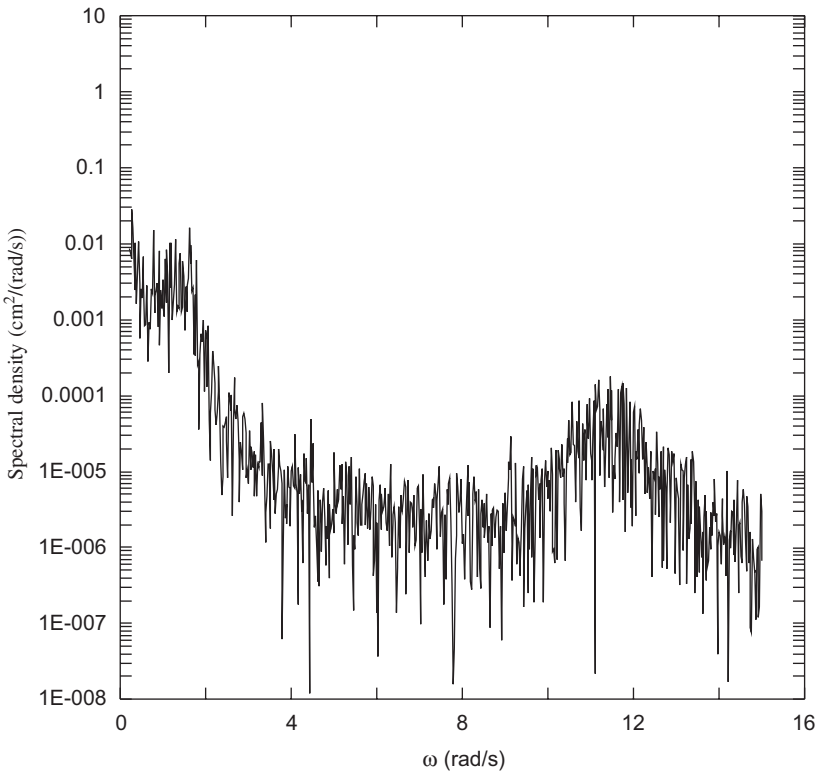

Fig. 12. *Y*-displacement spectrum based on Fig. 10 (noise-like vibration).

6. Modelling the instability

In this section the experimental observations are compared with predictions of different theories. All current theories in the literature, known to the authors of this paper, are not able to predict a complex motion that consists of two alternating types: a nearly periodic orbital motion and a noise-like vibration. For comparison between the experiment and theories, we first focus on the critical velocity and the frequency of the orbital motion at near-critical fluid velocities. To enable a meaningful comparison, all material and fluid parameters had to be carefully identified. In order to do so a few additional tests were carried out.

First, the elasticity modulus and the material damping in the pipe were identified. To this end, the dry pipe, i.e. hanging in air and without fluid inside, was given an initial deflection and then released. From the record of the pipe displacements, the period and decrements of free decaying vibrations were extracted. For this particular case, the motion of the free-hanging pipe in a plane is assumed to be described by the following equation of motion:

$$EI\frac{\partial^4 w}{\partial z^4}-\frac{\partial}{\partial z}\left(\rho_p A_p g(L-z)\frac{\partial w}{\partial z}\right)-\alpha\frac{\partial^3 w}{\partial z^2\,\partial t}+m_p\frac{\partial^2 w}{\partial t^2}=0 \tag{8}$$

in which ρ_f is the density of the pipe material, A_p the cross-sectional area of the pipe wall, L the length of the pipe, α the material damping coefficient and m_p the mass of the pipe per unit length. The material damping is taken proportional to the pipe curvature.

As a second step, the same free vibration tests were carried out with the cantilever pipes partly submerged in water and completely filled with still water. The added mass coefficient was determined from the measured period of vibration. From the decrement of vibrations, making use of the previously determined material damping, the hydrodynamic drag coefficients were calculated. The equations of motion in one plane for this situation, neglecting the internal underpressure in the pipe, applicable to the above-water and submerged parts, are given as

$$\begin{aligned}&EI\frac{\partial^4 w}{\partial z^4}-\frac{\partial}{\partial z}\left(\{\rho_p A_p g(L-z)-\rho_f A_p g(L-L_{\mathrm{dry}})-\rho_f A_i g(z-L_{\mathrm{dry}})\}\frac{\partial w}{\partial z}\right)\\&\quad-\alpha\frac{\partial^3 w}{\partial z^2\,\partial t}+(m_p+m_f)\frac{\partial^2 w}{\partial t^2}=0,\quad 0\leqslant z\leqslant L_{\mathrm{dry}},\end{aligned} \tag{9}$$

$$\begin{aligned}&EI\frac{\partial^4 w}{\partial z^4}-\frac{\partial}{\partial z}\left((\rho_p-\rho_f)A_p g(L-z)\frac{\partial w}{\partial z}\right)-\alpha\frac{\partial^3 w}{\partial z^2\,\partial t}+(m_p+m_f+m_a)\frac{\partial^2 w}{\partial t^2}\\&\quad+D_0\left(\frac{\mu}{D_0}A_1\frac{\partial w}{\partial t}+\frac{1}{2}\rho_f A_2\left|\frac{\partial w}{\partial t}\right|\frac{\partial w}{\partial t}\right)=0,\quad L_{\mathrm{dry}}<z\leqslant L,\end{aligned} \tag{10}$$

in which L_{dry} is the length of the pipe in air, ρ_f the density of the fluid, A_i the internal cross-sectional area of the pipe, m_f the mass of the internal fluid per unit length and m_a the added mass per unit length defined as

$$m_a=C_a\rho_f(A_p+A_i)$$

with C_a the added mass coefficient. From these auxiliary experiments without internal flow, the added mass coefficient C_a and the hydrodynamic drag coefficient A_1 were identified. The value obtained for the coefficient A_1, indicating the amount of linear viscous fluid damping, was smaller than predicted by Kuiper et al. (2007). The reason is that the parameter A_1 was estimated in that paper for a Stokes parameter $\beta=D_0^2/(\upsilon T)\approx 10^6$, while in our experiments the Stokes parameter was about 10^3. In the above expression, T is the period of oscillation and υ is the kinematic viscosity of the water.

The parameter A_2, related to the external drag, cannot be estimated from the auxiliary-free vibration experiments described above. Therefore, since this coefficient does not depend on the Stokes parameter, the value proposed by Kuiper et al. (2007) was used. Obviously, the latter parameter has no influence on the onset of instability.

For both pipes, all measured and calculated parameters are summarized in Table 2. The measured Y-displacement at the balcony level after releasing the pipe from an initial deflection and the corresponding theoretical prediction (with fitted parameters) based on Eqs. (9) and (10) are shown in Fig. 13 as an example.

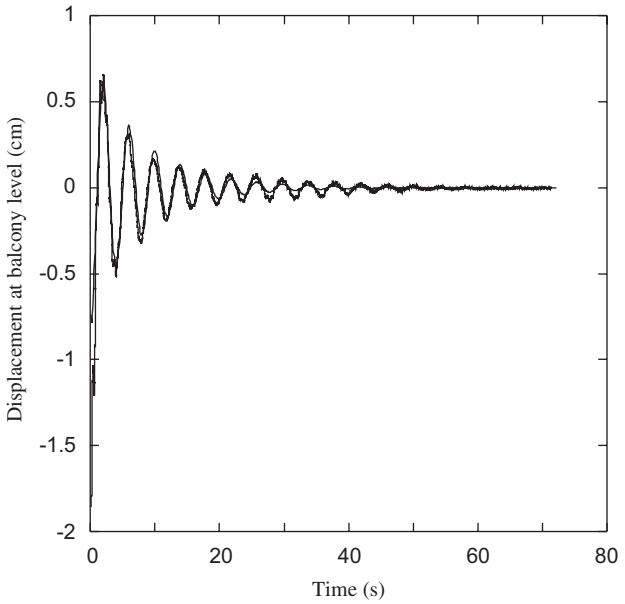

Fig. 13. Measured (bold line) and theoretical prediction (thin line) of Y-displacement of the pipe in the free vibration auxiliary test.

After identifying all parameters, the onset of instability could be theoretically calculated. To this end, the equations of motion for the pipe without fluid flow, Eqs. (9) and (10), were extended with fluid flow dependent terms:

$$EI\frac{\partial^4 w}{\partial z^4}-\frac{\partial}{\partial z}\left(\left\{\rho_p A_p g(L-z)-\rho_f A_p g(L-L_{\mathrm{dry}})-\rho_f A_i g(z-L_{\mathrm{dry}})+\frac{1}{2}\rho_f A_i u_f^2(-1+\gamma_e)\right\}\right)\frac{\partial w}{\partial z}$$
$$-2m_f u_f\frac{\partial^2 w}{\partial z\,\partial t}-\alpha\frac{\partial^3 w}{\partial z^2\,\partial t}+(m_p+m_f)\frac{\partial^2 w}{\partial t^2}=0,\quad 0\leqslant z\leqslant L_{\mathrm{dry}},\tag{11}$$

$$EI\frac{\partial^4 w}{\partial z^4}-\frac{\partial}{\partial z}\left(\left\{(\rho_p-\rho_f)A_p g(L-z)+\frac{1}{2}\rho_f A_i u_f^2(-1+\gamma_e)\right\}\frac{\partial}{\partial z}\right)-\alpha\frac{\partial^3 w}{\partial z^2\,\partial t}$$
$$-2m_f u_f\frac{\partial^2 w}{\partial z\,\partial t}+(m_p+m_f+m_a)\frac{\partial^2 w}{\partial t^2}+D_0\left(\frac{\mu}{D_0}A_1\frac{\partial w}{\partial t}+\frac{1}{2}\rho_f A_2\left|\frac{\partial w}{\partial t}\right|\frac{\partial w}{\partial t}\right)=0,\quad L_{\mathrm{dry}}<z\leqslant L.\tag{12}$$

The coefficient γ_e indicates the pressure loss at the entrance, varying between 0 for a smooth bell mouth inlet and 1 for a square-cut inlet.

In order to calculate the onset of instability, the boundary conditions should be known. At the top, the pipe is assumed to be fixed. As mentioned before, at the free entrance the bending moment is zero and for the balance of transverse forces two options are analysed:

$$EI\frac{\partial^3 w}{\partial z^3}-\alpha\frac{\partial^2 w}{\partial z\,\partial t}=0\quad\text{at}\quad z=L,\tag{13}$$

$$EI\frac{\partial^3 w}{\partial z^3}-\alpha\frac{\partial^2 w}{\partial z\,\partial t}-m_f u_f\frac{\partial w}{\partial t}=0\quad\text{at}\quad z=L.\tag{14}$$

These two boundary conditions are similar to Eqs. (4) and (6), except that the effect of the material damping is included. The third option for the balance of shear forces, Eq. (5), is not considered, since this, in contrast to the experiments, would predict divergence but not flutter.

Before the nonlinear equations, Eqs. (11) and (12), are solved in the time domain, the onset of instability predicted by the linear equations is determined by using the Argand diagram. Terms related to the nonlinear part of the hydrodynamic drag and the effective tension of the riser are disregarded in Eqs. (11) and (12). The key difference with Section 2 is that in this section the partly submerged pipe is considered instead of the fully submerged pipe. To obtain the Argand diagrams, the values corresponding to the smaller pipe diameter (see Table 2) are used. In Figs. 14 and 15

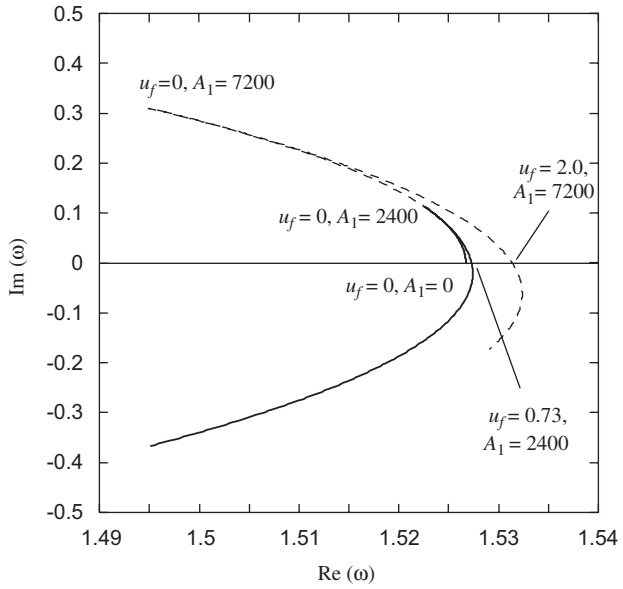

Fig. 14. Argand diagram for partly submerged pipe according to boundary condition (13). The regular line represents $A_1 = 2400$ and dotted line represents $A_1 = 7200$.

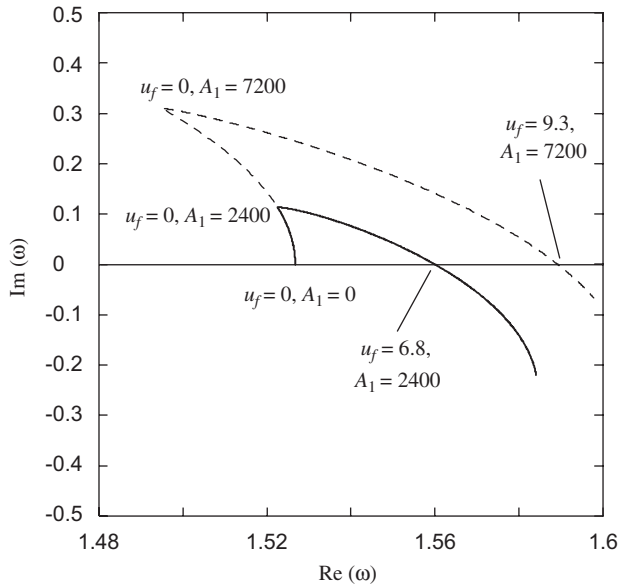

Fig. 15. Argand diagram for partly submerged pipe according to boundary condition (14). The regular line represents $A_1 = 2400$ and dotted line represents $A_1 = 7200$.

the paths of the first natural frequency are plotted as they depend on the linear damping coefficient and the fluid velocity. Fig. 14 is obtained using the conventional boundary condition at the free inlet, Eq. (13), while Fig. 15 is based on boundary condition (14). As explained above, the linear part of the hydrodynamic damping is not so easy to determine since it depends on the Stokes number. To investigate the sensitivity of the critical velocity to the linear damping, the paths of the first natural frequency have been plotted for both the measured linear damping coefficient ($A_1 = 2400$) and a three times larger value ($A_1 = 7200$). Obviously, a larger damping coefficient results in a larger critical velocity.

For the *conventional boundary condition* at the free inlet, Eq. (13), and using the parameters of the smaller pipe, the theoretical critical velocity is 0.73 m/s, while the experiments showed an onset of instability at velocities between 2.1 and 2.4 m/s. The experimentally observed critical velocity would only be predicted using a much higher linear damping

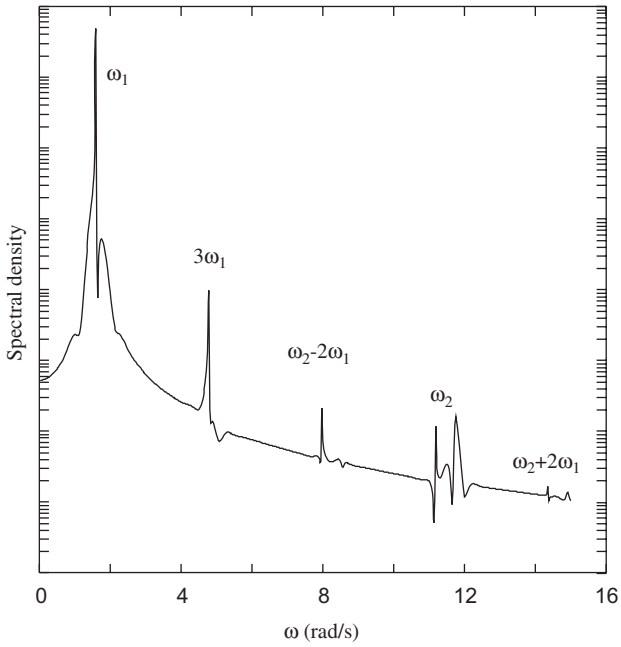

Fig. 16. Predicted displacement spectrum for an internal fluid velocity of $u_f = 3.6$ m/s. The pipe is subject to the conventional boundary condition, Eq. (13).

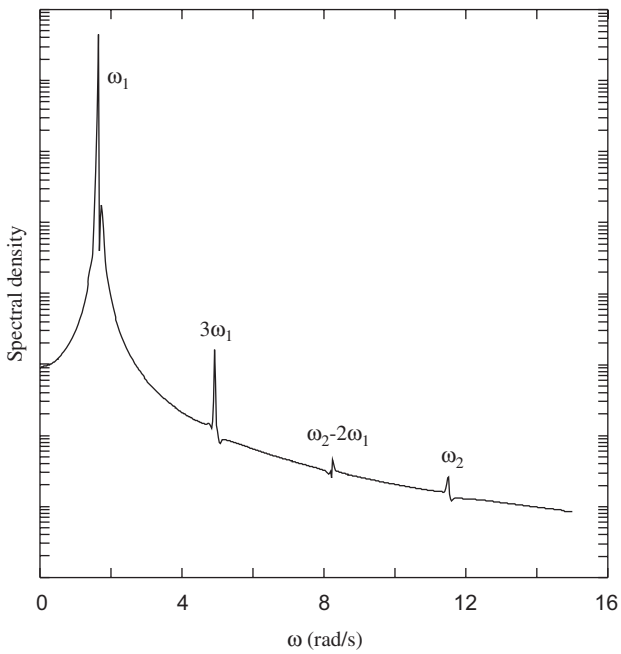

Fig. 17. Predicted displacement spectrum for an internal fluid velocity of $u_f = 9.0$ m/s. The pipe is subject to the boundary condition (14).

coefficient than measured (see the dotted line in Fig. 14). Besides, it is interesting to check whether the theoretical model captures the frequency at near-critical velocities. In the experiments the first natural frequency increased with fluid velocity from 1.5 rad/s at zero fluid velocity to 1.6 rad/s at near-critical fluid velocity. With measured frequency at near-critical velocities we mean the dominating frequency during orbital motion. This increase of frequency is in qualitative agreement with Fig. 14 but does not agree with it quantitatively.

Using the *boundary condition proposed by Païdoussis and co-authors*, Eq. (14), the onset of flutter for the smaller diameter pipe is at 6.8 m/s (Fig. 15), which is much larger than observed in the experiments. Also in this case the theory predicts an increase in the real part of the frequency with increasing fluid velocity from zero to near-critical. Again this is in qualitative agreement with the observations.

For the larger diameter pipe the same trend is observed. The experiments showed an onset of instability at velocities between 1.9 and 2.2 m/s. The conventional boundary condition predicts an onset at 0.56 m/s, whereas the boundary condition proposed by Païdoussis and co-authors predict an onset at 7.1 m/s.

In order to analyse the post-critical regime the nonlinear equations, Eqs. (11) and (12), were solved in the time domain. In these equations only the nonlinear hydrodynamic drag was accounted for to limit the structural vibrations. In the experiments it was observed that the displacements were relatively small, and hence, geometrical nonlinearities were neglected.

The equations of motion, Eqs. (11) and (12), and the boundary conditions are discretized using a second-order central difference approximation. The length of the riser L is divided into N segments, all having a length $h = L/N$. The first node is at $x = 0$ and the $(N+1)$th node at $x = L$. This yields a system of $(N+1)$ second-order differential equations, resulting in a system of $2(N+1)$ first-order ordinary differential equations.

In the post-critical regime both boundary conditions, Eqs. (13) and (14), predict finite amplitude oscillations, i.e. a limit cycle, due to the nonlinear drag. A spectrum of the calculated pipe displacement in the post-critical regime is shown in Fig. 16. The purpose of calculating this spectrum is to check whether the predicted dominant frequencies coincide with the measured ones. Since it is much more difficult to predict correctly the amplitude of motion, we skipped the values on the vertical axis. This figure is obtained using the conventional boundary condition, Eq. (13), and an arbitrarily chosen internal fluid velocity of $u_f = 3.6$ m/s. The spectrum is determined for the pipe displacement at the balcony level in order to compare calculations (Fig. 16) with measurements (Fig. 11). Obviously, the comparison is limited to the situation when the pipe orbits. The locations of the calculated and measured peaks agree quite well. According to the model, both the first and second mode are unstable, whereas the measurements show only first mode instability. Due to the nonlinear drag, peaks in the calculated spectrum arise additionally at $3\omega_1$, $\omega_2 - 2\omega_1$ and $\omega_2 + 2\omega_1$. Especially, the location of the measured peak around 4.8 rad/s (Fig. 11) coincides nicely with the prediction ($3\omega_1$).

A similar spectrum is plotted in Fig. 17 for the boundary condition proposed by Païdoussis and co-authors, Eq. (14). To be in the post-critical regime a much higher internal fluid velocity was needed. To this end $u_f = 9.0$ m/s was chosen in computations. For this fluid velocity the second mode was not yet unstable. In these computations, additional peaks were observed as well, originating from the nonlinear hydrodynamic damping. Again, the calculated and measured peak frequencies agree quite well.

By using two coupled equations in the two transverse directions, similar to Eqs. (1) and (2), one can successfully find an orbital motion with a finite amplitude. In the experiments, however, the instability was observed in the form of a complex motion that consists of two alternating parts: nearly periodic orbital motion with maximum amplitude of 1.5 times the pipe diameter and noise-like vibration with small deflections. Therefore, it can be concluded that there are still discrepancies between theory and experiments for both the onset of instability and the behaviour in the post-critical regime. In the next section some possibilities are examined which might explain these discrepancies. However, if one would imagine a model in which the boundary condition for the horizontal force switches in time between the descriptions given by Eqs. (13) and (14), one would come remarkably close to the measurements.

7. Possible explanations for the experimentally observed pipe behaviour

Existing theories do not predict: (i) the correct magnitude of the critical fluid velocity, (ii) the relatively long period that the pipe needs to start orbiting, (iii) the unsteady unstable motion that consists of an orbital motion alternating with a noise-like vibration, (iv) the amplitude of the steady-state orbital motion.

We attempted to improve existing models, to simulate the observed behaviour of the experimental pipe. Although a great deal of ideas was investigated, only two modelling attempts are addressed below.

In all the above-mentioned models the fluid flow velocity in the pipe was assumed to be constant. However, at the high fluid velocities attained in the experiments, the flow might have a pulsating character. This might result in an

additional vibration in the longitudinal direction of the system, which may affect the pipe motion in the transverse direction through parametric resonance. This could explain why the pipe needs so much time to start oscillating in the unstable regime. For a parametrically excited system, the first-order instability zone is located around $\Omega = 2\omega_0$, where Ω is the frequency of the parametric excitation and ω_0 is an eigenfrequency of the system. From the measured data we observed that the pipe vibrates only at the first natural frequency, which is about 2 rad/s. The parametric excitation, i.e. the pulsating fluid flow, to be able to perceptibly affect the transverse motion, should show a peak in the fluid velocity spectrum around 4 rad/s. The measurements do not show any peak around this frequency. The same holds for lower excitation frequencies which could lead to higher-order parametric instability zones. Hence, parametric resonance is not likely to occur in our experimental set-up.

As explained in Section 2, the correct description of the flow field in the vicinity of the tip is of great importance for the stability of the pipe conveying fluid. The complex inflow is largely simplified by the boundary condition at the tip of the pipe. To improve the boundary condition at the free inlet, a model was developed in which the inclination at the free end of the pipe ($\partial w/\partial x_{x=L}$) relative to the angle of inflow (ϕ) was not prescribed but introduced as a degree of freedom. This was done by introducing a "pipe tail" representing the part of the inflow below the inlet, as shown in Fig. 18. This part lags behind the inlet due to interaction with the surrounding water. The boundary condition at the free end for this situation is

$$EI\frac{\partial^3 w}{\partial z^3} - \alpha\frac{\partial^2 w}{\partial t\,\partial z} - m_f u_f^2\left(-\frac{\partial w}{\partial z} + \phi\right) = 0 \quad \text{at} \quad z = L. \tag{15}$$

An additional pendulum equation was added to describe the motion of the "tail". After analyzing this system, it became clear that the term $m_f u_f(\partial w/\partial t)$ in the boundary condition, which is absent in Eq. (15), is the dominating factor for stability rather than the angle of inflow. More research is being currently carried out in this direction.

Thus, at the moment we cannot explain the observed behaviour of the cantilever pipe in full detail. After analysing the experiments, a few possible explanations could not be verified, since not everything was measured. For example, it is unclear whether the internal fluid flow undergoes a swirling motion instead of the assumed axial fluid motion. Besides, it was not measured whether the pipe rotates about its axis during the experiments. All these shortcomings will be addressed in a new set of experiments, which are currently being planned. The influence of the tank wall, if present, will

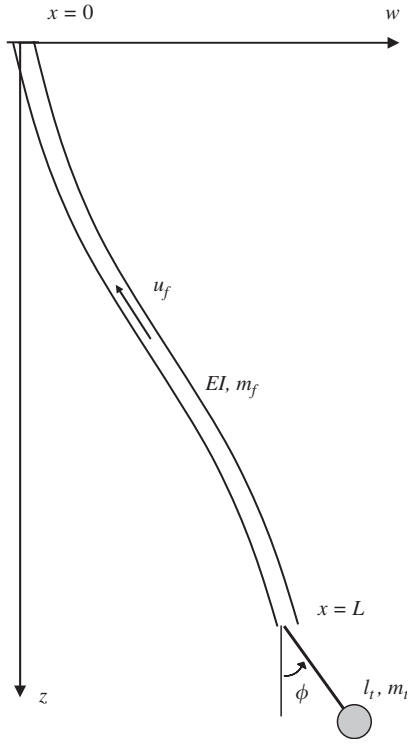

Fig. 18. Sketch of a cantilever pipe with a free angle of inflow.

be greatly reduced by moving the pipe toward the middle of the tank. As an important next step, different types of inlet pieces will be examined, like a smooth bell-shaped mouthpiece, a piece with a sloping end, etc.

8. Conclusion

For the first time, it was experimentally proven that a partly submerged cantilever pipe aspirating water becomes unstable beyond a critical internal fluid velocity. Below this velocity the system is stable, whereas above it the system shows a complex motion that consists of two alternating phases: nearly periodic orbital motion and noise-like vibration with very small amplitudes. Increasing the internal fluid velocity results in an increasing amplitude of the orbital pipe motion. In these experiments the maximum displacement amplitude was a few pipe diameters.

Existing theories predict the dominant frequencies quite well. However, they do not correctly predict the critical velocity and the pipe behaviour in the unstable regime. It seems that the flow field in the vicinity of the tip is of great importance for the correct prediction of the dynamic behaviour of the cantilever pipe conveying fluid. Soon, new experiments with the pipe in the middle of the tank will be carried out, using different inlet pieces, to investigate the effect of the flow field further.

Acknowledgements

This research is supported by the Technology Foundation STW, Applied Science Division of NWO and the technology programme of the Dutch Ministry of Economic Affairs. We thank WL Delft Hydraulics for their great support in building the experimental set-up and helping us during the experiments. In particular, the excellent cooperation with M. Boele and T. Ammerlaan is highly appreciated. We also thank Professor J.A. Battjes for his valuable comments on this paper.

References

Hongwu, C., Junji, T., 1996. Effect of boundary conditions on the stability of a cantilever pipe discharging and aspirating fluid. JSME International Journal Series C 39, 20–24.

Kuiper, G.L., Metrikine, A.V., 2005. Dynamic stability of a submerged, free hanging riser conveying fluid. Journal of Sound and Vibration 280, 1051–1065.

Kuiper, G.L., Metrikine, A.V., Battjes, J.A., 2007. A new time-domain drag description and its influence on the dynamic behaviour of a cantilever pipe conveying fluid. Journal of Fluids and Structures 23, 429–445.

Païdoussis, M.P., 1998. Fluid–Structure Interactions: Slender Structures and Axial Flow, vol. 1. Academic Press, London.

Païdoussis, M.P., 1999. Aspirating pipes do not flutter at infinitesimally small flow. Journal of Fluids and Structures 13, 419–425.

Païdoussis, M.P., 2005. Some unresolved issues in fluid–structure interactions. Journal of Fluids and Structures 20, 871–890.

Païdoussis, M.P., Luu, T.P., 1985. Dynamics of a pipe aspirating fluid, such as might be used in ocean mining. ASME Journal of Energy Resources Technology 107, 250–255.

Païdoussis, M.P., Semler, C., Wadham-Gagnon, M., 2005. A reappraisal of why aspirating pipes do not flutter at infinitesimal flow. Journal of Fluids and Structures 20, 147–156.